 Nucleic Acids Research, 1999, Vol. 27, No. 23 **4619–4625**

Global structure similarities of intact and nicked DNA complexed with IHF measured in solution by fluorescence resonance energy transfer

Mike Lorenz, Alexander Hillisch, Steven D. Goodman[1] and Stephan Diekmann*

Department of Molecular Biology, Institute for Molecular Biotechnology, PO Box 100813, D-07708 Jena, Germany and [1]Department of Biological Sciences, University of Southern California School of Dentistry, Los Angeles, CA 90089-0641, USA

Received August 6, 1999; Revised and Accepted October 7, 1999

ABSTRACT

We have analyzed the structure of two related protein–DNA complexes consisting of integration host factor (IHF) bound to two different versions of the H′ site of bacteriophage λ. Both DNA substrates were 55 bp in length. While one was native duplex the other possessed a nick in one strand at a crucial position within the IHF consensus at the same position as in the reported crystal structure of the DNA–IHF complex. By labeling the 5′-ends of these DNA molecules with donor and acceptor fluorescent dyes, we were able to measure the distance between the dyes by fluorescence resonance energy transfer (FRET) and model DNA distortion. The FRET efficiency decreased from 0.49 ± 0.01 (nicked DNA) to 0.37 ± 0.01 (intact DNA) when the gap in the DNA strand was closed. The measured dye-to-dye distance of IHF in complex with nicked DNA was in agreement with the expected value from the crystal structure. Although we found that the two structures were distinguishable, the global shape induced by IHF was retained between the two DNA molecules. Furthermore, our FRET and modeling techniques have sufficiently high resolution to distinguish subtle changes in nucleoprotein complexes with biological relevance.

INTRODUCTION

Higher as well as lower organisms contain proteins which are present in many copies per cell and serve as multipurpose architectural elements. The integration host factor (IHF) and the histone-like HU protein are closely related prokaryotic proteins, bending the DNA and thus helping to bring together multiple components of higher order complexes (for reviews see 1,2).

The *Escherichia coli* IHF was originally identified (3–6) and purified (7) as a host factor for the phage λ integrative recombination reaction. Subsequently, IHF was shown to regulate a large number of DNA–protein interactions, including stimulation of transcription of some σ54 and σ70 promoters, as first demonstrated for the *nif* operon of *Klebsiella pneumoniae* (8,9), stabilization of repressor binding (10) and enhancement of transposition (11–13). IHF also influences the initiation of DNA replication, as it is frequently a component of the multiprotein complex which forms at bacterial origins of replication (14; reviewed in 15–17). The role of IHF can be mimicked by replacing one or more IHF binding sites with intrinsically curved DNA (18) or by replacing IHF with a different DNA-bending protein (HU) (19).

IHF binds selectively to phage attachment sites (attP) and to specific sequences within IHF-responsive promoters. IHF protects more than 25 bp. However, only 9 bp, found in two patches on the 'right' site (3′-downstream) of the binding site, show significant sequence conservation (20). Through comparison of native IHF-binding sites, a degenerate core sequence has been defined that consists of three elements: two clusters of conserved base pairs (5′-WATCAA-3′) and (5′-TTR-3′) and a dA/dT-rich element located one helical turn 5′-upstream. Although the upstream element is not found at all sites, it has been shown to enhance the binding of IHF (21,22).

IHF is a small heterodimeric, sequence-specific DNA-binding protein of homologous α and β subunits of ~10 kDa each. The two subunits are 30% sequence identical. IHF binds in the minor groove of the DNA causing it to bend in a sequence-specific manner (2,23). Two sharp kinks in the DNA are caused by the intercalation of conserved prolines from each arm of the dimer. The intercalated proline residues interrupt base pair stacking and cause the minor groove to open on either side of the center of the bend. The intertwined α and β subunits of the IHF dimer contact the bent DNA in a roughly symmetrical manner. However, protein contacts to the conserved bases of the right half of the binding site are extensive and intimate, whereas the dA/dT element on the left half of the complex is contacted via direct and water-mediated interactions with the DNA phosphates. Both subunits stabilize the DNA bend around the protein by electrostatic interactions with the DNA backbone.

A theoretical model of IHF places the arms of the protein in the minor groove, wrapping around the DNA (24,25). The backbone protection pattern for the H′ site suggests that the two kinks have a similar shape (25).

*To whom correspondence should be addressed at: Institut für Molekulare Biotechnologie, Beutenbergstraße 11, D-07745 Jena, Germany. Tel: +49 3641 656260; Fax: +49 3641 656261; Email: diekmann@imb-jena.de

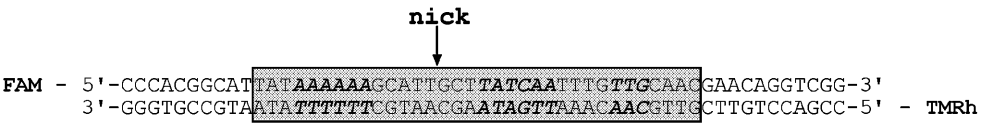

Figure 1. Sequence of the 55 bp long DNA molecules containing the H′ site of phage λ. The dyes fluorescein (FAM) and tetramethylrhodamine (TMRh) are coupled to the 5′-ends of the strands via a C_6 linker. The position of the nick in the molecule is indicated and the DNA bases essential for IHF binding are shown in bold. The DNA complexed to IHF in the crystal (23) is indicated by the shaded box.

The extent of DNA bending induced by IHF in solution has been estimated by gel mobility analysis to be >140° (26). DNA cyclization experiments indicate that the bending angle is closer to 180° than to 120° (27). In the crystal the DNA is bent to ~160° (23).

The capacity of IHF to contort DNA into a virtual U-turn represents a great structural feat. The solution of the co-crystal structure of IHF bound to one of its DNA targets adds greatly to our understanding of how this protein-induced manipulation is performed. One of the limitations of this co-crystal generated structure was the authors use of a nicked DNA substrate. In the crystal structure the DNA contains a nick positioned at one of the two kinking sites, opening the helix to the extent (in the crystal structure 16 Å, allowing some local rearrangement of at least 7.5 Å) that the gap cannot be bridged by a phosphate linkage. Thus, to close the linkage the DNA structure must be modified. We speculated that the structure of the complex with nicked DNA might differ from the global solution structure with intact DNA. A change in global structure should result in a different end-to-end distance of the DNA. We therefore determined the end-to-end distance of the intact and the nicked DNA complexed with IHF in solution by measuring the distance-dependent fluorescence resonance energy transfer (FRET) between two dye molecules covalently attached to the DNA helix ends.

MATERIALS AND METHODS

Preparation of fluorescence-labeled DNA sequences

The oligonucleotides containing the H′ site of phage λ as a sequence-specific IHF-binding site (Fig. 1) were synthesized as described elsewhere (28).

The intact double-stranded DNA was annealed by hybridizing equal amounts of complimentary fluorescein- and rhodamine-conjugated or non-labeled 55 bp oligonucleotides in 450 mM NaCl, 2 mM $MgCl_2$, 24 mM sodium citrate (pH 7.0) by slow cooling from 80 to 4°C overnight. For the nicked DNA the rhodamine-conjugated 55 bp oligonucleotide was first hybridized with a 31 bp non-labeled oligonucleotide by slow cooling from 80 to 20°C, and in a second step hybridized with a 24 bp fluorescein-conjugated single strand by slow cooling from 60 to 4°C overnight.

Duplex DNA molecules were purified by 10% native polyacryamide gel electrophoresis, cut out of the gel under UV illumination and extracted by high salt electroelution with 3 M ammonium acetate at 4°C.

The buffer of the DNA samples were changed to protein binding buffer (100 mM NaCl, 20 mM Tris–HCl, pH 7.9, 1 mM EDTA) on a Sephadex G25 column. Absorption measurements of these solutions were made from 240 to 650 nm to determine the concentration of the samples and to control the quantity of labeling. The DNA absorption coefficient used was $\varepsilon_{DNA}(260\ nm) = 675\ 000\ M^{-1}\ cm^{-1}$ (estimated from the 50 μg/unit method) and gives $\varepsilon_{FAM}(490\ nm) = 60\ 000\ M^{-1}\ cm^{-1}$ and $\varepsilon_{TMRh}(560\ nm) = 75\ 000\ M^{-1}\ cm^{-1}$ for the conjugated dyes. While ε_{TMRh} was not significantly affected by conjugation, ε_{FAM} was decreased compared to the values observed for the free dye, as reported by Clegg *et al.* (29). The values indicate 100% labeling of the intact DNA with both fluorescent dyes and 100% labeling of the nicked DNA with the acceptor tetramethylrhodamine (TMRh) and 89% with the donor fluorescein (FAM). This reduced labeling efficiency was corrected for in the data analysis (see Materials and Methods, FRET).

Spectroscopic studies

Absorption and fluorescence measurements were taken on a Specord M500 (Zeiss, Germany) and a SLM 48000S instrument (SLM Aminco, Urbana, IL). Steady-state fluorescence spectra were corrected for lamp fluctuation. Polarization artifacts were avoided by using 'magic angle' conditions. The fluorescence samples were excited at 490 nm for the FRET spectra and at 560 nm for the acceptor spectra. The fluorescence spectra were collected over a broad range of emission wavelength from 500 to 650 nm and from 570 to 650 nm and corrected for buffer signals. Aliquots of 400 μl of ~150 nM intact or nicked DNA were titrated with a 12 μM IHF stock solution up to a final IHF concentration of ~450 nM and incubated for 10 min for each titration step. All measurements were carried out at 15°C and repeated three times with different DNA samples. Treatment of the molecules and data aquisition and handling were carried out as described by Stühmeier *et al.* (30).

DNA melting curves of intact and nicked DNA were obtained with a Varian Cary 4E UV-VIS spectrophotometer. The absorbance at 260 nm was measured over the range 30–90°C with a heating rate of 2°C/min. The DNA solution buffer was the same as the protein binding buffer. Under these conditions the melting points of the DNA molecules were determined as 84°C for the intact and 74°C for the nicked DNA. For both DNAs just one transition could be observed. The melting points were calculated by the first derivative method using the computer program Thermal v.1.0 from Varian.

Fluorescence anisotropies *r* were calculated from fluorescence intensity measurements by a vertical excitation polarizer with vertical ($F_{\parallel}$) and horizontal ($F_{\perp}$) emission polarizers according to

$$r = (F_{\parallel} - G \cdot F_{\perp})/(F_{\parallel} + 2 \cdot G \cdot F_{\perp})$$

with the experimental correction factor $G = F_{\perp}/F_{\parallel}$ (31).

Fluorescence resonance energy transfer (FRET)

The efficiency of fluorescence resonance energy transfer E from a fluorescence donor to an acceptor is related to the donor–acceptor distance R according to

$$E = R_0^6/(R_0^6 + R^6)$$

R_0 is the Förster distance at which the energy transfer efficiency is 50%, calculated from

$$R_0 = 9790\cdot(J\kappa^2\phi_D n^{-4})^{1/6}\ \text{Å}$$

where J is the spectral overlap integral of the dyes, ϕ_D the quantum yield of the donor in absence of the acceptor, n the refraction index of the medium and κ^2 the orientation of the transition dipole moments (32–34). For rapid randomization of the relative donor–acceptor orientation κ^2 is 2/3 (35). The low anisotropies of the donor fluorescein implies that this is a good approximation for this study (29), so that the efficiency of energy transfer E is sensitive only to the donor–acceptor distance R.

The emission intensity of the donor decreases in the presence of FRET and the intensity of the acceptor emission correspondingly increases. Therefore we determined the energy transfer efficiency E once from quenching of the donor emission fluorescence intensity in the presence of acceptor (by binding IHF) according to

$$E = (I_D - I_{DA})/I_D = (I_{DNA} - I_{complex})/I_{DNA}$$

where I_D and I_{DA} are the intensities of the donor-only (no energy transfer) and the donor–acceptor samples, respectively. Usually, I_D and I_{DA} are measured in independent experiments. We determined both values within one experimental set-up by adding protein to the DNA solution and thus avoiding pipetting errors. Due to separation of the donor from the acceptor dye in space, no energy transfer takes place in the labeled protein-free DNA and the donor emission intensity of the free DNA equals that of the donor-only sample $I_D = I_{DNA}$. $I_{complex}$ corresponds to I_{DA}. $I_{complex}$ and I_{DNA} are obtained by integrating the fluorescence intensities from 505 to 525 nm for the complex and free DNA, respectively.

In addition, the FRET efficiency E was determined by measuring the intensity of the sensitized emission of the acceptor normalized to the fluorescence of the acceptor alone (36).

$$(\text{ratio})_A = [F(\lambda_{em},490) - a\cdot F^D(\lambda_{em},490)]/F(\lambda_{em},560)$$
$$= E\cdot d^+\cdot(\varepsilon^{D,490}/\varepsilon^{A,560}) + (\varepsilon^{A,490}/\varepsilon^{A,560})$$

$(\text{ratio})_A$ is linearly dependent on the efficiency of energy transfer, E. It normalizes the measured sensitized FRET signal for the concentration, for the quantum yield of the acceptor and for any errors in percentage of acceptor labeling. $F(\lambda_{em},490)$, $F(\lambda_{em},560)$ and $F^D(\lambda_{em},490)$ are the fluorescence spectra of donor and acceptor labeled and donor-only labeled DNA samples excited at the given wavelength of 490 or 560 nm, respectively. ε^D and ε^A are the molar absorption coefficients of the donor and acceptor at the given wavelength. d^+ is the fraction of donor labeled molecules, calculated from the absorption spectrum of the doubly labeled DNA molecule.

Observing the DNA binding and bending of IHF by electrophoretic mobility shift assay

Different concentrations of IHF were incubated for 15 min at 20°C with doubly labeled intact and nicked DNA (400 nM) in 100 mM NaCl, 20 mM Tris–HCl (pH 7.9) and 1 mM EDTA. The samples were loaded on a native 8% polyacryamide gel and electrophoresed for 100 min at 80 V in 1× TBE buffer (100 mM Tris, 83 mM borate, 1 mM EDTA, pH 8.0). The gels were directly scanned using a FluorImager 595 (Molecular Dynamics) and analyzed with the ImageQuaNT software and visualized with FluorSep from Molecular Dynamics. The DNA was excited with an argon laser at 488 nm and the fluorescence detected in the ranges 515–545 nm (using a 530DF30 filter) and 575–605 nm (590DF30 filter).

Modeling of IHF

The model of the nicked 55 bp DNA in complex with IHF was built by fitting double helical B-form DNA fragments to the last 4 bp of each DNA end in the crystal structure.

A model of the intact DNA complexed with IHF was built based on the crystal structure of IHF in complex with a 35 bp target DNA fragment containing a nick in one of the kinked sites (23). The DNA conformation of this complex is characterized by the nicked DNA strand showing a distance of ~16 Å between the 5′-phosphate and 3′-ribose oxygen of the unconnected nucleotides. In order to obtain a starting structure for the model with intact DNA, we replaced the kinked site containing the nick with the intact kinked site in the crystal complex.

Thus, the non-nicked DNA of one half-site of the complex was extracted and superimposed on the nicked half-site in the stem 2 region. The ends of the DNA strands were joined. The new DNA half-site exhibited very similar contacts to the protein, however, due to the modified DNA conformation, the β-hairpin of the β subunit lost many close contacts to the minor groove of the DNA. Thus, this loop (His54–Val77) was modified to correspond to the protein monomer binding to intact DNA in the crystal. The sequence of the modeled DNA was changed to the sequence depicted in Figure 1. Double helical B-form DNA fragments were fitted to the last 4 bp, to extend the DNA ends as shown in Figure 1. General molecular modeling operations were performed with SYBYL v.6.4 (37).

The resulting model was energy optimized using the AMBER 91 force field (38) within AMBER v.4.1 (39), keeping all backbone atoms in the protein fixed except for the two hairpin loops. A distance-dependent dielectric function of $\varepsilon = 4r$ (where r is the distance between two interacting atoms in Å) was used. A residue-based 'twin-range' cut-off of 10/15 Å was applied for the treatment of non-bonded interactions (39). During the first 100 optimization steps, a steepest descent minimization was performed. The energy optimization was then switched to the conjugate gradient method and terminated when the gradient norm of successive steps was <0.1 kcal/(mol Å).

Modeling of the dye position at the DNA ends

The distribution of dye positions at the DNA helix ends were calculated taking into account their steric and electronic properties derived from *ab initio* calculations. A systematic conformational search with the AMBER 91 force field involving all rotatable bonds of the dye molecules and its C6 amino linkers was carried out, resulting in well-defined spatial regions that in principle represent the population of different dye conformers on the DNA helix ends. The majority of the 6-FAM conformers are pointing away from the DNA with an extended linker conformation. This is presumed to be mainly due to electrostatic repulsion between the 2-fold negatively charged

dye and the polyanionic DNA. In contrast, the majority of the zwitterionic 5-TMRh conformers interact with the DNA in the major groove and stack on top of the DNA helix (40). The results of these calculations are in agreement with experimental data obtained in anisotropy (41) and burst-integrated fluorescence lifetime (BIFL) (42) experiments. Anisotropy measurements indicate that 6-FAM freely rotates in solution, whereas 5-TMRh interacts with the DNA. BIFL experiments show direct contacts of TMRh with the last base pair (C.Seidel, personal communication). Taking the theoretical calculations and experimental data together, it seems likely that 5-TMRh stacks on top of the DNA helix end.

RESULTS

The DNA complexed by IHF adopts a U shape. We analyzed a 55 bp DNA–IHF complex with, in the center, the H′ protein binding site from λ phage (Fig. 1). Both arms of the U shape are made up of two turns of DNA while the kink distance is 9 bp. The binding sequence is identical to that analyzed in crystals by Rice *et al*. (23). The 5′-ends of the DNA were labeled with the fluorescent dyes FAM and TMRh. The DNA arms of two turns length place the dyes distant from the protein so that interactions between dyes and IHF protein can be excluded (Fig. 6). The exact length of the two DNA arms were designed such that the distance between the two dyes was in the range of R_0 (50 Å), the distance with the highest sensitivity of FRET. The positions of the dyes at the helix ends obtained from theoretical calculations were used for these purposes.

The anisotropies *r* of the donor FAM and the acceptor TMRh were determined and increased for both dyes only slightly in the complex compared to the free DNA (from ~0.06 to 0.10 for FAM and from ~0.25 to 0.27 for TMRh). This increase is explained by the Perrin equation. The volume *V* of the complex is larger than the volume of the free DNA and the fluorescence lifetime of the donor τ decreases when energy transfer takes place. An interaction between the dyes and the protein would result in steric hindrance of dye rotation and thus in reduced rotational diffusion. This would result in a strong effect on the anisotropies, much larger than that observed experimentally. This supports our conclusion that the protein does not interact with the dye molecules.

In the complex, the DNA helix ends are sufficiently close to one another in space that Förster transfer takes place between the dyes. The intensity of FRET is inversely proportional to the sixth power of the distance between the dyes and allows estimation of the end-to-end distance of the DNA double helix.

Two different DNA molecules were studied: one with an intact double helix and a second containing a nick in the FAM-labeled strand (Fig. 1). A 35 bp long DNA molecule with the nick at the same position had been co-crystallized with IHF and the structure analyzed (23). We determined the end-to-end distance of the intact and the nicked DNA complexed with IHF in solution. The principle of the measurement is displayed in Figure 2.

Electrophoretic mobility shift assay

The doubly labeled DNA complexed with IHF was analyzed in native 8% polyacrylamide gels (Fig. 3). Gel electrophoretic mobility shift separates the naked DNA from the DNA–protein complex. The gel was analyzed using a FluorImager. The

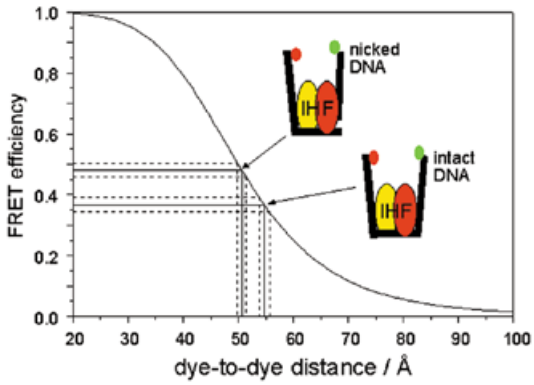

Figure 2. Principle of experimental approach. The FRET efficiency is inversely proportional to the sixth power of the dye-to-dye distance. The end-to-end distance of the nicked DNA in the complex is smaller compared to the end-to-end distance of the intact DNA, resulting in a larger FRET efficiency.

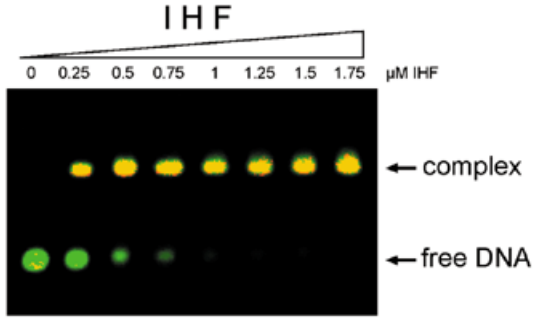

Figure 3. Native 8% polyacrylamide gel of the intact DNA and the DNA–IHF complex. Aliquots of 400 nM of fluorescein and rhodamine labeled DNA as shown in Figure 1 were incubated with increasing concentrations of IHF protein as indicated and electrophoresed. The resulting gel was analyzed with a Fluoro-Imager. The DNA was excited at 488 nm and the fluorescence detected in the ranges 515–545 (green fluorescence) and 575–605 nm (red fluorescence). The free unbound DNA, where no energy transfer can be observed, shows a green fluorescence. In the complex the dyes are sufficiently close to one another to induce energy transfer. Therefore the green fluorescence from the donor decreases while the red fluorescence from the acceptor increases; this results in a yellow band for the DNA–IHF complex.

DNA/ fluorescein donor was excited at 488 nm. The free DNA emits green light detected in the range 515–545 nm, while the DNA–IHF complex shows a yellow color. In the complex the dye molecules at the helix ends come close to one another in space and induce Förster transfer. Energy will be transferred from the donor to the acceptor dye, reducing the donor and increasing the acceptor emission intensity. The acceptor emits at higher wavelengths and can be detected in the range 575–605 nm (red), resulting in yellow bands (a mixture of green donor and red acceptor fluorescence) for the DNA–IHF complex. The decreasing intensity of the donor emission and the increasing acceptor fluorescence (Fig. 3) indicate a strong FRET efficiency and thus a close DNA end-to-end distance in the DNA–protein complex.

Naked as well as protein-bound DNA migrates more slowly in polyacrylamide gels when curved or bent. This migration

anomaly becomes maximal when the curve/bend is in the center of the DNA (as in the analyzed molecules). We compared the mobility of IHF complexed to nicked and intact DNA in a native 8% polyacrylamide gel (data not shown). The gel did not show migration differences between the two DNA–IHF complexes. Thus, the bending angles of nicked and intact DNA complexed with IHF are similar.

Fluorescence resonance energy transfer (FRET)

We measured the FRET between the dye molecules at the DNA helix ends for the intact and nicked DNA free of protein as well as in complex with IHF in solution by measuring the reduction in donor and increase in acceptor emission. The first method compares the donor emission intensities of a sample without energy transfer (naked DNA) with the same amount of a donor–acceptor sample (IHF-bound DNA), where energy from the excited donor can be transferred to an acceptor molecule. The donor emission of the donor–acceptor sample decreases due to energy transfer. The second method determines the FRET efficiency by measuring the intensity of the sensitized acceptor emission normalized to the fluorescence of the acceptor alone.

In the free DNA, no energy transfer was observed when measuring sensitized acceptor emission (Method 2). The helix ends are at a distance of ~200 Å beyond the range where FRET can be observed. Adding IHF to intact as well as to nicked DNA results in a conformational change of the DNA structure. As a consequence, the helix ends are brought close to one another in space and energy transfer takes place. For the intact DNA a FRET efficiency of 0.37 ± 0.01 and for the nicked DNA of 0.49 ± 0.01 was measured in three independent experiments.

With increasing IHF concentration, the donor fluorescence decreases in both cases. Figure 4 shows the donor fluorescence spectra for different IHF concentrations normalized relative to the donor fluorescence in the absence of IHF. With increasing IHF concentration, the reduction in donor fluorescence levels off at 300 nM IHF. The reduced levels of donor fluorescence at high IHF concentrations are 63 ± 2 and 52 ± 2% of the value for free intact and nicked DNA, respectively. This gives a FRET efficiency of 0.37 ± 0.02 for the intact and of 0.48 ± 0.02 for the nicked DNA (Fig. 5). The FRET efficiencies measured by (i) decreasing donor and (ii) increasing acceptor fluorescence agree well within the error limits of the experiments (Table 1).

Quenching of the donor fluorescence in the presence of IHF protein can be excluded. In parallel experiments with donor-only samples, the donor fluorescence intensity was constant (data not shown). Therefore, the decreasing donor fluorescence was caused by energy transfer to the acceptor dye.

From the FRET efficiency, the dye distance can be calculated. With the Förster distance R_0 of 50 Å (28,43) the measured FRET efficiency values yield dye distances of 54.7 Å for the intact and 50.5 Å for the nicked DNA (Table 1). The dye distances increased by ~4 Å when the nick in the DNA complexed with IHF was closed.

Binding constants

From IHF concentration-dependent complex formation, the binding constants of IHF complexed to intact and nicked DNA were determined in solution (Fig. 5). The IHF binding constants are 9 ± 1 and 5 ± 1 nM for intact and nicked DNA at 15°C and agree within an order of magnitude with reported values (24,44) obtained by different experimental methods. The binding free energies are –44.4 ± 0.3 and –45.8 ± 0.5 kJ/mol. This corresponds to a release of 1.4 ± 0.6 kJ/mol strain energy for the nicked DNA compared to the intact DNA.

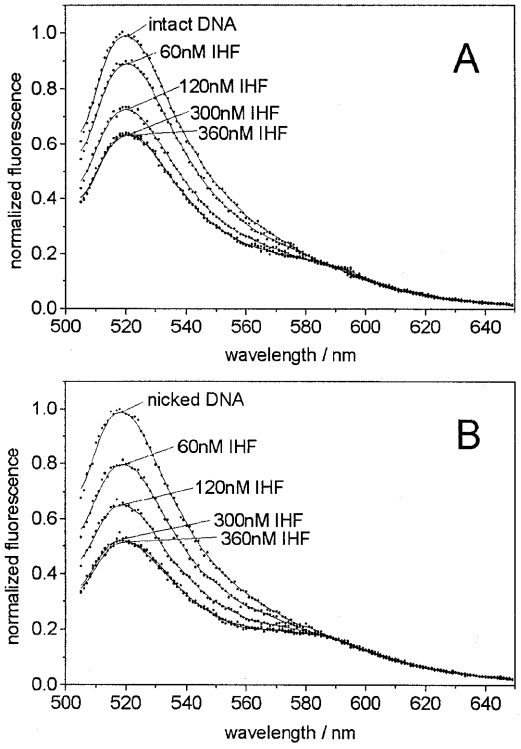

Figure 4. Fluorescence spectra for free DNA and complexed with increasing concentrations of IHF. (**A**) Intact DNA; (**B**) nicked DNA. The fluorescence is normalized relative to the fluorescence of the protein-free DNA. With increasing concentration of IHF the donor fluorescence intensity decreases to 63 ± 2 and 52 ± 2% of the intensity of free DNA, resulting in FRET efficiencies of 0.37 ± 0.02 and 0.48 ± 0.02 for intact and nicked DNA, respectively.

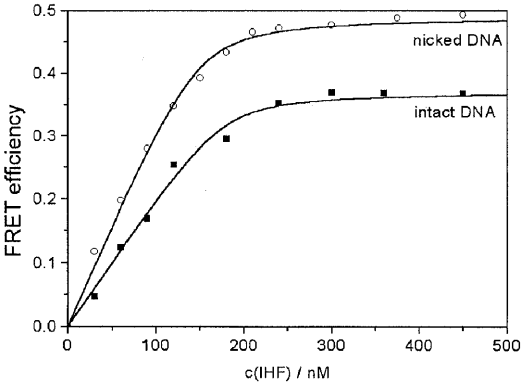

Figure 5. FRET efficiency versus IHF concentration for nicked and intact DNA. With increasing IHF concentration the FRET efficiency levels off to 0.37 ± 0.02 and 0.48 ± 0.02 for intact and nicked DNA. Therefore the dye-to-dye distances for the DNA–IHF complexes with intact and nicked DNA are 54.7 ± 1.1 and 50.7 ± 1.0 Å, respectively. The determined IHF binding constants to intact and nicked DNA in solution are 9 ± 1 and 5 ± 1 nM, respectively.

Table 1. Measured and calculated dye-to-dye distances of the DNA helix ends in DNA–IHF complexes in solution

	Intact DNA	Nicked DNA
Measured by decreasing donor fluorescence		
FRET efficiency[a]	0.37 ± 0.02	0.48 ± 0.02
Distance (Å)[b]	54.7 ± 1.1	50.7 ± 1.0
Measured by increasing acceptor fluorescence		
$(ratio)_A$[a]	0.39 ± 0.01	0.45 ± 0.01
FRET efficiency[c]	0.37 ± 0.01	0.49 ± 0.01
Distance (Å)[b]	54.6 ± 0.5	50.3 ± 0.3
Calculated with molecular modeling		
Distance (Å)	56 ± 4	51 ± 4

[a]Errors are standard deviations of three independent measurements.
[b]Calculated with a Förster constant R_0 of 50 Å (28,43).
[c]FRET efficiencies were calculated from the $(ratio)_a$ value with $\varepsilon^{A,490}/\varepsilon^{A,560}$ 0.095 and $\varepsilon^{D,490}/\varepsilon^{A,560}$ 0.8 (43); d^+ for the intact DNA is 1 and for the nicked DNA 0.89 (see Materials and Methods).

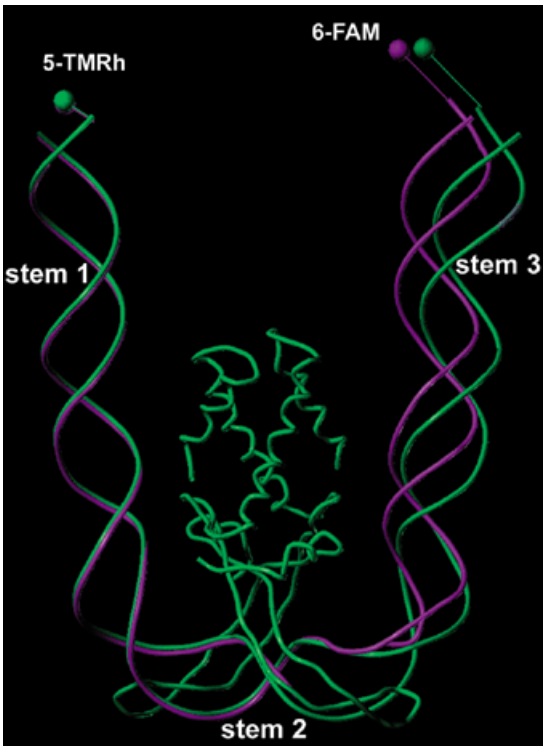

Figure 6. Comparison of the global structure of the intact (green) and nicked (violet) DNA–IHF complex. The positions of the dyes are indicated by spheres in the respective color of the molecules. 5-TMRh appears on the left side and 6-FAM on the right side of the picture.

DISCUSSION

Proteins that bind DNA likely alter their DNA target. While these changes can be subtle, some proteins, like IHF, create such dramatic deformations that there are specific and necessary functional consequences. Since many nucleoprotein complexes consist of multiple proteins bound to a single DNA target, it becomes increasingly important to be able to resolve each distinct complex and to determine the contribution of each protein to each specific structure.

The recently solved crystal structure of a 35 bp DNA fragment and IHF adopts a U shape with two sharp kinks separated by 9 bp. In construction of the DNA substrate the authors relied on a DNA molecule with a single nick rather than a completely intact duplex. Since the nick is involved in crystal packing, crystals of a complex with intact DNA could not be obtained (23). Unfortunately, the nick appears at the position of one of the two kinks that IHF is believed to generate upon binding. All base pairs in the crystal were Watson–Crick base pairs, with the exception of the two dA/dT base pairs at the nick, which form a Hoogsteen configuration or form a reverse Watson–Crick base pair. The distance between the 5′-phosphate and the 3′-ribose oxygen of the base pairs flanking the gap is ~16 Å. The two dA residues in the nicked kink have the same symmetry as the two dA residues in the other 'intact' kink. Therefore we could remove this artifact of the Hoogsteen and reverse Watson–Crick pairing and form 'normal' Watson–Crick pairs by replacing the nicked kink with both dA/dT pairs from the 'intact' kink. The distance from the 5′-phosphate to the 3′-ribose oxygen now becomes 7.5 Å. A normal phosphate–oxygen binding length is 1.6 Å and therefore the gap cannot be bridged by a phosphate linkage. Thus, the intact DNA in the complex must have an at least slightly modified structure.

This variation is not evident during electrophoretic mobility shift assay when IHF is complexed with either nicked or intact DNA substrates. In this current work, we used the higher resolution FRET technique to determine structural differences between the complexes and to provide sufficient data to create more refined models of binding. Altered FRET efficiencies can be induced by differences in the bending angle and/or by un- or overwinding of the DNA.

Using the crystal structure as a starting point, we constructed models of the nicked and intact DNA bound to IHF. The distance between the two dyes in the model of the nicked complex exactly matched the experimental data (Table 1). The model of the intact DNA bound to IHF was built by replacing the nicked kink site with the intact site and adjusting the position of stem 3 according to the FRET measurements. The model shows how an intact continuous DNA substrate could be bound to IHF. These structures have a similar global appearance (Fig. 6) showing, however, some specific differences. In the complex with intact DNA the double helix leaves the nicked kink with a different rise. The bases are shifted with a rise of ~1.5 Å, the overall twist of the DNA is smaller and the DNA bending angle is ~2° smaller compared to the crystal structure. This leads to a different orientation of stem 3 with respect to stem 1 (Fig. 6). The FRET efficiency between the dyes at the helix ends is sufficiently sensitive to detect this structural difference. Indeed, the energy transfer between the dyes is decreased by 12% when the gap in the DNA is closed, indicating that the helix end-to-end distance of the DNA–IHF complex increases by ~4 Å, from 50.5 to 54.7 Å. The overall bending angles in both complexed structures are similar, as indicated by the gel migration data. Both values agree well with one another.

The model indicates that the intact DNA shows a slightly different structure within the second kink. Nevertheless, the global structure is hardly changed. The reason for this might be that the IHF binds to the DNA not only between and at the two kinked sites but also outside the kinks holding the DNA in position. We thus speculate that the global DNA structure only weakly depends on the detailed DNA structure at the kink sites.

In conclusion, we have shown that our FRET technique adds significantly to the solved structure of IHF bound to a DNA target. This methodology is of high enough resolution to distinguish even subtle changes in DNA architecture. Since IHF and other DNA bending proteins are often accessory factors in multiprotein–DNA complexes, this technique should prove useful in revealing both gross and fine structural variations in the resulting DNA structures, a first step in elucidating the contribution of DNA architecture to function.

ACKNOWLEDGEMENTS

We thank the Deutsche Akademische Austauschdienst (DAAD) and the British Research Council for support and A. A. Travers for helpful discussions.

REFERENCES

1. Ellenberger,T. and Landy,A. (1997) *Structure*, **5**, 153–157.
2. Rice,P.A. (1997) *Curr. Opin. Struct. Biol.*, **7**, 86–93.
3. Williams,J.G.K., Wulff,D.L. and Nash,H.A. (1977) In Bukhari,A., Shapiro,J. and Adhya,S. (eds), *DNA Insertion Elements, Plasmids and Episomes*. Cold Spring Harbor Laboratory Press, Cold Spring Harbor, NY, pp. 357–361.
4. Miller,H.I., Kikuchi,A., Nash,H.A., Weisberg,R.A. and Friedman,D.I. (1979) *Cold Spring Harbor Symp. Quant. Biol.*, **43**, 1121–1126.
5. Miller,H.I., Mozola,M.A. and Friedman,D.I. (1980) *Cell*, **20**, 721–729.
6. Nash,H.A., Mizuuchi,K., Enquist,L.W. and Weisberg,R.A. (1981) *Cold Spring Harbor Symp. Quant. Biol.*, **45**, 417–428.
7. Nash,H.A. and Robertson,C.A. (1981) *J. Biol. Chem.*, **256**, 9246–9253.
8. Hoover,T.R., Santero,E., Porter,S. and Kustu,S. (1990) *Cell*, **63**, 11–22.
9. Kustu,S., Santero,E., Keener,J., Popham,D. and Weiss,D. (1989) *Microbiol. Rev.*, **53**, 367–376.
10. Betermier,M., Rousseau,P., Alazard,R. and Chandler,M. (1995) *J. Mol. Biol.*, **249**, 332–341.
11. Signon,L. and Kleckner,N. (1995) *Genes Dev.*, **9**, 1123–1136.
12. Leung,P.C., Teplow,D.B. and Harshey,R.M. (1989) *Nature*, **338**, 656–658.
13. Mizuuchi,M. and Mizuuchi,K. (1989) *Cell*, **58**, 399–408.
14. Hwang,D.S. and Kornberg,A. (1992) *J. Biol. Chem.*, **267**, 23083–23086.
15. Friedman,D.I. (1988) *Cell*, **55**, 545–554.
16. Freundlich,M., Ramani,N., Mathew,E., Sirko,A. and Tsui,P. (1992) *Mol. Microbiol.*, **6**, 2557–2563.
17. Goosen,N. and van de Putte,P. (1995) *Mol. Microbiol.*, **16**, 1–7.
18. Goodman,S.D. and Nash,H.A. (1989) *Nature*, **341**, 251–254.
19. Goodman,S.D., Nicholson,S.C. and Nash,H.A. (1992) *Proc. Natl Acad. Sci. USA*, **89**, 11910–11914.
20. Goodrich,J.A., Schwartz,M.L. and McClure,W.R. (1990) *Nucleic Acids Res.*, **18**, 4993–5000.
21. Hales,L.M., Gumport,R.I. and Gardner,J.F. (1994) *J. Bacteriol.*, **176**, 2999–3006.
22. Hales,L.M., Gumport,R.I. and Gardner,J.F. (1996) *Nucleic Acids Res.*, **24**, 1780–1786.
23. Rice,P.A., Yang,S., Mizuuchi,K. and Nash,H.A. (1996) *Cell*, **87**, 1295–1306.
24. Yang,S.W. and Nash,H.A. (1994) *Proc. Natl Acad. Sci. USA*, **91**, 12183–12187.
25. Yang,C.C. and Nash,H.A. (1989) *Cell*, **57**, 869–880.
26. Thompson,J.F. and Landy,A. (1988) *Nucleic Acids Res.*, **16**, 9687–9705.
27. Sun,D., Hurley,L.H. and Harshey,R.M. (1996) *Biochemistry*, **35**, 10815–10827.
28. Lorenz,M., Hillisch,A., Payet,D., Buttinelli,M., Travers,A. and Diekmann,S. (1999) *Biochemistry*, **38**, 12150–12158.
29. Clegg,R.M., Murchie,A.I., Zechel,A., Carlberg,C., Diekmann,S. and Lilley,D.M. (1992) *Biochemistry*, **31**, 4846–4856.
30. Stühmeier,F., Hillisch,A., Clegg,R.M. and Diekmann,S. (1999) *Synthesis, Purification and Physical Measurement of FRET in DNA*. Oxford University Press, in press
31. Lakowicz,J.R. (1983) *Principle of Fluorescence Spectroscopy*. Plenum Press, New York, NY.
32. Clegg,R.M. (1996) In Wang,X.F. and Herman,B. (eds), *Fluorescence Imaging Spectroscopy and Microscopy*. John Wiley & Sons, New York, NY, pp. 179–252.
33. Förster,T. (1948) *Ann. Phys.*, **2**, 55–75.
34. Van der Meer,B.W., Coker,G. and Chen,S.-Y.S. (1994) *Resonance Energy Transfer—Theory and Data*. VCH, New York, NY.
35. Förster,T. (1949) *Z. Naturforsch.*, **4A**, 321–327.
36. Clegg,R.M. (1992) *Methods Enzymol.*, **211**, 353–388.
37. Tripos (1997) SYBYL v.6.4. Tripos Inc., St Louis, MO.
38. Weiner,S.J., Kollman,P.A., Nguyen,D.T. and Case,D.A. (1986) *J. Comp. Chem.*, **7**, 230–252.
39. Pearlman,D.A., Case,D.A., Caldwell,J.W., Ross,W.S. and Cheatham,T.E. (1995) AMBER Version 4.1. University of California, San Francisco, CA.
40. Hillisch,A. (1998) Thesis, University of Vienna, Vienna, Austria.
41. Vamosi,G., Gohlke,C. and Clegg,R.M. (1996) *Biophys. J.*, **71**, 972–994.
42. Eggeling,C., Fries,J.R., Brand,L., Gunther,R. and Seidel,C.A. (1998) *Proc. Natl Acad. Sci. USA*, **95**, 1556–1561.
43. Stühmeier,F., Welch,J.B., Murchie,A.I., Lilley,D.M. and Clegg,R.M. (1997) *Biochemistry*, **36**, 13530–13538.
44. Wang,S., Cosstick,R., Gardner,J.F. and Gumport,R.I. (1995) *Biochemistry*, **34**, 13082–13090.